

RESEARCH ARTICLE

Swelling compensation of engineered vasculature fabricated by additive manufacturing and sacrifice-based technique using thermoresponsive hydrogel

Xue Yang^{1†}, Shuai Li^{2†*}, Xin Sun^{3†}, Ya Ren¹, Lei Qiang⁴, Yihao Liu³, Jinwu Wang^{3,5*}, Kerong Dai^{1,3*}

¹College of Medicine, Southwest Jiaotong University, No. 144 Jiada Road, Chengdu 610031, People's Republic of China

²Department of Orthopedics, The First Affiliated Hospital, Zhejiang University School of Medicine, No. 79 Qingchun Rd, Hangzhou 310003, People's Republic of China

³Shanghai Key Laboratory of Orthopedic Implants, Department of Orthopedic Surgery, Shanghai Ninth People's Hospital, Shanghai Jiao Tong University School of Medicine, No. 639 Zhizaoju Rd, Shanghai 200011, People's Republic of China

⁴School of Materials Science and Engineering, Southwest Jiaotong University, No. 111 2nd Ring Rd, Chengdu 611756, People's Republic of China

⁵Med-X Research Institute, School of Biomedical Engineering, Shanghai Jiao Tong University, No. 1956 Huashan Rd, Shanghai 200030, People's Republic of China

†These authors contributed equally to this work.

***Corresponding authors:**

Shuai Li (allenle1991@sina.com)

Jinwu Wang

(wangjw-team@shsmu.edu.cn)

Kerong Dai

(krdai@163.com)

Citation: Yang X, Li S, Sun X, *et al.*, 2023, Swelling compensation of engineered vasculature fabricated by additive manufacturing and sacrifice-based technique using thermoresponsive hydrogel. *Int J Bioprint*, 9(5): 749. <https://doi.org/10.18063/ijb.749>

Received: January 31, 2023

Accepted: March 2, 2023

Published Online: May 10, 2023

Copyright: © 2023 Author(s).

This is an Open Access article distributed under the terms of the Creative Commons Attribution License, permitting distribution, and reproduction in any medium, provided the original work is properly cited.

Publisher's Note: Whioce Publishing remains neutral with regard to jurisdictional claims in published maps and institutional affiliations.

Abstract

Engineered vasculature is widely employed to maintain the cell viability within *in vitro* tissues. A variety of fabrication techniques for engineered vasculature have been explored, with combination of additive manufacturing with a sacrifice-based technique being the most common approach. However, the size deformation of vasculature caused by the swelling of sacrificial materials remains unaddressed. In this study, Pluronic F-127 (PF-127), the most widely used sacrificial material, was employed to study the deformation of the vasculature. Then, a thermoresponsive hydrogel comprising poly(N-isopropylacrylamide) (PNIPAM) and gelatin methacrylate (GelMA) was used to induce volume shrinkage at 37°C to compensate for the deformation of vasculature caused by the swelling of a three-dimensional (3D)-printed sacrificial template, and to generate vasculature of a smaller size than that after deformation. Our results showed that the vasculature diameter increased after the sacrificial template was removed, whereas it decreased to the designed diameter after the volume shrinkage. Human umbilical vein endothelial cells (HUVECs) formed an endothelial monolayer in the engineered vasculature. Osteosarcoma cells (OCs) were loaded into a hierarchical vasculature within the thermoresponsive hydrogel to investigate the interaction between HUVECs and OCs. New blood vessel infiltration was observed within the lumen of the engineered vasculature after *in vivo* subcutaneous implantation for 4 weeks. In addition, engineered vasculature was implanted in a rat ischemia model to further study the function of engineered vasculature for blood vessel infiltration. This study presents a small method aiming to accurately create engineered vasculature by additive manufacturing and a sacrifice-based technique.

Keywords: Swelling compensation; Engineered vasculatures; Additive manufacturing; Sacrificial materials; Thermoresponsive hydrogels

1. Introduction

Mammalian vasculature consists of two connected and highly branched networks that pervade human body and have a significant influence on pathophysiology^[1,2]. Tissue engineering is involved in many fields^[3–5]. In the past two decades, the generation of living model tissues containing engineered vasculature has been among the main research topics within the fields of biomanufacturing and tissue engineering. Vasculature facilitates the diffusional mass transfer of nutrients, oxygen, growth factors, biochemical signaling factors, carbon dioxide, and metabolic waste from the surroundings to cells and vice versa^[6,7]. The success of engineered tissues largely depends on the incorporation of stable vasculature that assists the various biological functions of encapsulated cells. Moreover, the engineered tissues containing vasculature enable enhanced cell infiltration and uniform distribution of nutrients and oxygen, which further augments cellular infiltration rates and host tissue integration compared to engineered tissues without vasculature^[8]. Therefore, fabricating engineered tissues with the incorporation of vasculature becomes critical. The development of a facile method to precisely fabricate engineered vasculature is still highly anticipated.

While robust whole-organ vascularization remains a major obstacle^[9], several techniques have been introduced to produce hydrogel constructs with vasculature. The most widely used strategies are three-dimensional (3D) bioprinting^[2], sacrifice-based technique^[10], and light-assisted processes^[11]. Among them, light-assisted processes, including digital light projection (DLP)^[12], volumetric printing^[13], and stereolithography^[14], empower the fabrication of engineered tissues with precise and complex vasculature. Grigoryan *et al.*^[15] used natural and synthetic food dyes as photoabsorbers that enable stereolithographic fabrication of hydrogel constructs containing intricate and functional vascular architectures, which could be a milestone in fabricating engineered vasculature. In their study, a bioinspired alveolar model with an ensheathing vasculature was successfully produced. Despite impressive progress, light-assisted processes require specific photoresponsive hydrogels. Moreover, high technical light-assisted equipment is essential for precisely fabricating target constructs, which makes light-assisted processes unscalable for researchers in tissue engineering and medicine. Another commonly used approach to fabricate engineered vasculature is combining additive

manufacturing and a sacrifice-based technique^[16]. In this method, first, a temporary sacrificial template in the shape of the designed vasculature is printed. Then, the sacrificial template is removed to form the engineered vasculature after encasing in a hydrogel construct. Currently, Pluronic F-127 (PF-127) and poly (vinyl alcohol) (PVA) occupy a leading position among sacrificial materials. Jennifer A. Lewis's lab was the pioneer to use PF-127 to produce vascularized tissues^[17–20]. More recently, to mimic a tumor microenvironment, Neufeld *et al.*^[21] printed PF-127 as the sacrificial template to create a vascularized glioblastoma model. However, deformation of the template was observed after removing the printed PF-127, decreasing the accuracy of the fabricated vasculature. The swelling of PF-127 may be caused by the hydrophilicity of F-127 at the removal temperature of 4°C^[22], which makes PF-127 absorb water from the surrounding environment. PVA is likewise an attractive sacrificial material for fabricating engineered vasculature due to its biocompatibility and water solubility. Nevertheless, the swelling of PVA in the hydrogel and the removal process, which are discernible, lead to vasculature deformation^[23]. Therefore, a specific coating is required to alleviate the swelling^[24,25]. While the combination of additive manufacturing and the sacrifice-based technique facilitates the fabrication of engineered vasculature, the deformation caused by swelling of the sacrificial template has been rarely studied.

Despite the flexibility of combining additive manufacturing and a sacrifice-based technique to fabricate engineered vasculature, it is also highly desirable to mitigate the deformation caused by swelling of the sacrificial template and develop a facile strategy for precisely preparing engineered vasculature within hydrogel constructs. Recently, the volume shrinkage of thermoresponsive hydrogel has been widely used for producing soft robotics and drug delivery carriers^[26–30]. In these studies, poly(N-isopropylacrylamide) (PNIPAM) is one of the most commonly adopted thermoresponsive hydrogels. PNIPAM exhibits a lower critical solution temperature (LCST) at ~32°C, which enables the volume shrinkage of PNIPAM in a cell culture environment^[31,32]. Wang *et al.*^[33] used the reversible shrinkage and swelling behavior of PNIPAM controlled by near-infrared irradiation to facilitate the penetration of endothelial cells into the bone scaffold vasculature and promote pre-vascularization. The scaffold vasculature enhances host vessel infiltration deep into the scaffolds. Nonetheless, the dimensions of the scaffold vasculature are uniform owing to the consecutive extrusion and printing of hollow fibers, which makes it difficult to prepare biomimetic vasculature. In our previous study, sacrificial alginate fibers and PNIPAM/gelatin methacrylate (GelMA) were combined

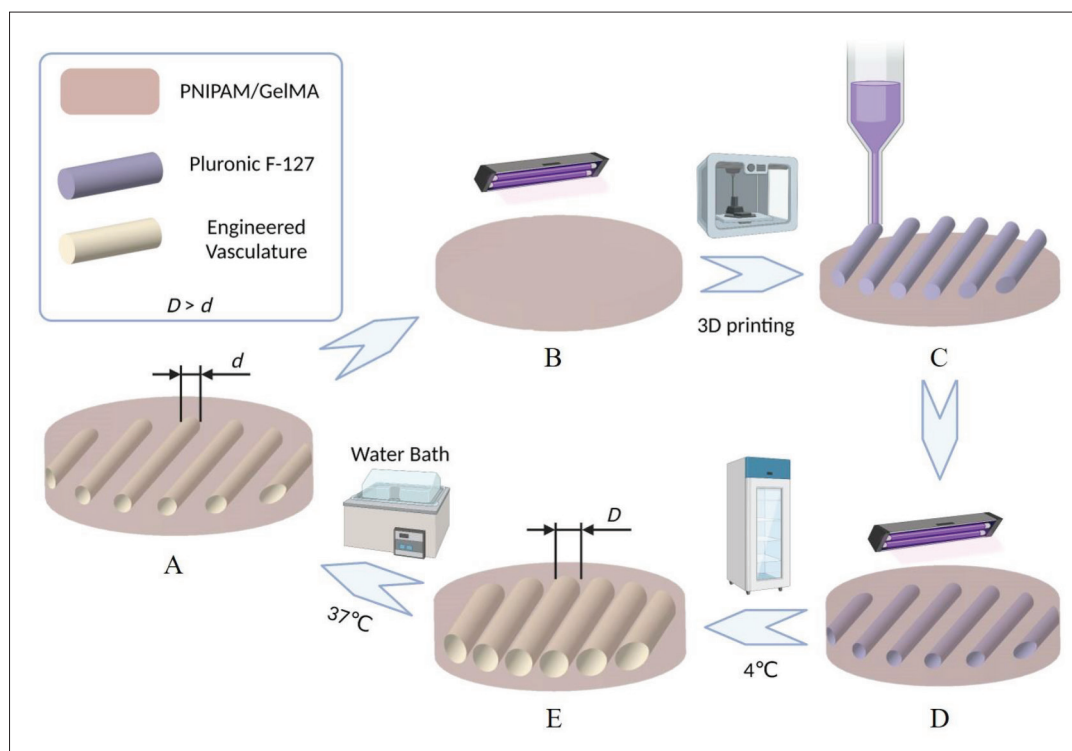


Figure 1. Schematic diagram of swelling compensation of vasculature fabricated by additive manufacturing and sacrifice-based technique using thermoresponsive hydrogel. (A) Hydrogel scaffold with vasculature at designed diameter d . (B) Fabrication of P/G hydrogel film. (C) 3D printing of sacrificial material on the P/G hydrogel film. (D) Encapsulation of the sacrificial template in the P/G hydrogel. (E) Engineered vasculature within the P/G hydrogel scaffold after swelling of the sacrificial template. Created with BioRender.com.

to generate micro-scale vasculature^[34]. The minimum vasculature diameter achieved is 50 μm . However, the study focused on fabricating micro-scale vasculature that is as small as possible. Moreover, the wet-spun alginate fibers of the sacrificial template are arbitrarily distributed, which makes it difficult to control the shape of the target vasculature.

Inspired by the volume shrinkage induced by the thermoresponsive hydrogel in the cell culture environment and the scalability of combining additive manufacturing and a sacrifice-based technique to fabricate engineered vasculature, we hypothesize that the volume shrinkage can compensate for the deformation caused by swelling of the sacrificial template. We established a molding mechanism for easy preparation of engineered vascular networks by varying the concentration of materials, density of vessels, and other factors to achieve precise preparation of engineered vasculature. Thus, the swollen vasculature within the hydrogel constructs can be tuned to the designed dimension to achieve precise manufacturing. Here, 3D printing and the sacrifice-based technique were combined to fabricate engineered vasculature through thermal post-treatment of the engineered vasculature at the cell culture temperature (37°C), fabricating vasculature

of a smaller size than the swollen one and thus enhancing the precision of the engineered vasculature, as shown in Figure 1. Vasculature with the diameter at d in hydrogel scaffold was designed (Figure 1A). For the precise fabrication of engineered vasculature, a PNIPAM/GelMA (P/G) hydrogel film was first generated, as shown in Figure 1B. As a proof of concept, PF-127 was used as the sacrificial material and printed on the P/G hydrogel film to form the sacrificial template, as shown in Figure 1C. Subsequently, freshly prepared P/G hydrogel was utilized to cover the sacrificial template, and the whole hydrogel scaffold was crosslinked under ultraviolet (UV) light to encapsulate the sacrificial template, as shown in Figure 1D. Then, the hydrogel scaffold with the sacrificial template was placed at 4°C to remove the sacrificial template to form the engineered vasculature. The swelling of the sacrificial template increased the engineered vasculature diameter from d to D (Figure 1E). Finally, the scaffold was placed at 37°C to induce the volume shrinkage of the thermoresponsive P/G hydrogel. After shrinking, the engineered vasculature with the targeted diameter at d was accomplished. The effects of different P/G concentrations and various vasculature densities on the precise fabrication of engineered vasculature were quantitatively explored.

Then, the flexibility in fabricating 3D engineered vasculature was verified by the 3D printing sacrificial template with multiple layers. HUVECs were cultured in the engineered vasculature to form the endothelial monolayer, and the biocompatibility of the engineered vasculature fabricated by our proposed method was tested. In addition, osteosarcoma cells (OCs) were loaded into a hierarchical vasculature within the thermoresponsive hydrogel to study the interaction between human umbilical vein endothelial cells (HUVECs) and OCs. P/G hydrogel scaffolds with vasculature were implanted into animals to study vascular infiltration and reconstruction within the vasculature.

2. Materials and methods

2.1. Materials and reagents

N-isopropylacrylamide (NIPAM) monomer and N,N'-methylenebisacrylamide (MBA) crosslinker were purchased from Aladdin, China. The photoinitiator, lithium phenyl-2,4,6-trimethylbenzoylphosphinate (LAP), sodium alginate (low viscosity), gelatin, and PF-127 were purchased from Sigma-Aldrich, USA. GelMA was purchased from Engineering For Life (EFL) at the Suzhou Intelligent Manufacturing Research Institute, China. In this study, 30 g PF-127 was dissolved in 100 mL ultrapure water to prepare the sacrificial PF-127 solution, unless otherwise indicated.

2.2. Swelling compensation for 3D-printed vasculature

A customized 3D printer based on a fused deposition modeling (FDM) printer (Tenlog, China) and syringe pump (Shengchen, China) was used to print the sacrificial materials. To print with precision, the sacrificial template with a designed diameter, 19-G (I. D. 720 μm , O. D. 1080 μm), 20-G (I. D. 610 μm , O. D. 910 μm), and 21-G (I. D. 520 μm , O. D. 820 μm) needles were used to print the zigzag structure. Different feed rates of the syringe pump were set to check the printability and diameters of the sacrificial templates. To preliminarily validate the hypothesis that the volume shrinkage of the P/G hydrogel can compensate for the swelling induced by the removal of the sacrificial template, the sacrificial PF-127 was printed on the P/G film. In this experiment, 10 wt% NIPAM, 0.15 wt% MBA, 3 wt% GelMA, and 0.075 wt% LAP were dispersed in ultrapure water homogeneously to prepare the P/G₃ solution. Then, 1.5 mL P/G₃ solution was transferred to a 35-mm Petri dish and polymerized under UV light at a distance of 10 cm for 20 s. After that, the polymerized P/G₃ hydrogel was placed on the receiving platform of the customized printer to print the zigzag sacrificial template. After printing, 1.5 mL P/G₃ solution was used to cover the

printed sacrificial template and polymerize it under UV light. The edge of the hydrogel scaffold was cut to expose the sacrificial template and placed at 4°C for 20 min to remove the sacrificial template. Subsequently, ultrapure water was gently injected to fully clear the engineered vasculature. Finally, the hydrogel scaffold with engineered vasculature was placed in a 35-mm Petri dish, which was left to float in a 37°C water bath to precisely fabricate the designed vasculature. The diameters of the printed sacrificial template and the channel at different times were measured under an optical microscope.

2.3. Effect of PNIPAM/GelMA (P/G) concentration on swelling compensation

To study the effect of P/G concentration on the precise fabrication of the engineered vasculature, P/G₁, P/G₃, and P/G₅ hydrogels were prepared. The composition of the P/G₁, P/G₃, and P/G₅ hydrogels is summarized in **Table S1** (Supplementary File). A 20-G needle was used in this section. The engineered vasculature was fabricated as the above protocol. Then, the hydrogel scaffolds with engineered vasculature shrunk at 37°C, and the change in areas and diameters of the vasculature was recorded. The diameter of the vasculature was measured under an optical microscope. The area of the P/G hydrogel scaffold was quantified using ImageJ software. The shrinkage ratio *SR* was computed using the following formula:

$$SR \times 100\% = \frac{A_1 - A_2}{A_1} \times 100\% \quad (1)$$

where A_1 was the area of the as-prepared P/G hydrogel scaffold, and A_2 was the hydrogel scaffold area after shrinking.

2.4. Effect of vasculature density on swelling compensation

To investigate the effect of vasculature density on volume shrinkage, three patterns of sacrificial templates were designed. Patterns 1, 2, and 3 have three, six, and nine fibers, respectively. P/G₂, P/G₃, and P/G₄ were used as the hydrogel concentrations, and a 20-G needle was utilized. After the removal of sacrificial templates, the scaffolds with different patterns of vasculature were placed at 37°C to record the diameters and areas at 0, 0.5, 1, 2, 3, 4, and 5 h. The shrinking ratio was calculated using **Equation 1**.

2.5. Fabrication of 3D vasculature

To fabricate 3D vasculature based on the proposed method in order to enhance the mass transfer, sacrificial templates with two, four, and six layers were designed. The images of engineered vasculature after dissolving and shrinking were captured. Red acrylic paint was injected into the engineered vasculature to show the 3D structure. P/G₃ was used as the hydrogel concentration, and a 20-G needle was utilized.

2.6. Characterization

The P/G hydrogels and PF-127 were measured by Fourier transform infrared spectroscopy (FTIR) to determine the presence of residual PF-127 in the prepared P/G hydrogels. To confirm the surface characteristics' changes of the P/G hydrogel at 25°C and 37°C, the contact angles were examined. The contact angle of the P/G hydrogel film at 25°C was measured directly by placing the film on the platform of the contact angle meter (JC2000D1, POWEREACH, China). After shrinking in a 37°C water bath for 2 h, the P/G hydrogel film was placed on a heating plate at the temperature of 37°C. The heating plate was transferred to the platform of the contact angle meter to measure the contact angle of the P/G hydrogel film at 37°C. The contact angles were captured immediately after dropping the water on the hydrogel samples to avoid the absorption. The surface of the vasculature within scaffolds fabricated by PF-127 and PF-127 + gelatin was observed by scanning electron microscopy (SEM, SIRION 200, USA). The samples were freeze-dried in liquid nitrogen and lyophilized, and the inner surface of the vasculature was sputtered with gold for observation using SEM. Compression modulus was measured with a mechanical tester (BAIROE, China) for the control group (no vascular scaffold), group I (1 × 1 scaffold), group II (4 × 4 scaffold), and group III (8 × 8 scaffold).

2.7. Formation of endothelial monolayer

Hydrogel scaffolds with engineered vasculature were used in this section to study the endothelialization of HUVECs. P/G₃ was used as the hydrogel concentration, and a 20-G needle was employed. Pattern 2 with six fibers was used to fabricate the samples. Cells up to passage 6 were used in the following experiments. The fabricated samples were immersed in 75% ethanol overnight under UV light, washed with phosphate-buffered saline (PBS; Cytiva, USA) thrice, shrank in the 37°C incubator for 30 min, and immersed in freshly prepared endothelial cell medium (ScienCell, USA) at 37°C before use. After trypsinization, the cells were resuspended in endothelial cell medium at a concentration of 2.5×10^6 cells/mL. Then, the cell suspension was slowly injected into the vasculature channels using a 1-mL sterilized syringe. After culturing in the incubator for 4 h, the samples were flipped upside down, and the cell suspension with the same concentration was injected into the vasculature again to achieve a uniform and complete cell seeding. Finally, the samples were statically cultured with the medium changed every day and observed under a microscope (Olympus, Japan). Fresh medium was injected into the channel gently to ensure the nutrient supply for cells. After culturing for 5 days, CD31 antibody, vinculin antibody, and vascular endothelial growth factor (VEGF) antibody immunostaining was performed on the hydrogel

scaffolds to investigate the intercellular connection and endothelialization function of the endothelial monolayer formed on the inner surface of the engineered vasculature. Samples were washed with pre-warmed PBS and fixed in 4% paraformaldehyde (BL539A, Biosharp, China) for 30 min at room temperature. Then, the samples were treated with 0.1% Triton X-100 (Triton X, Biosharp, China) diluted in PBS for 30 min. Subsequently, the scaffolds were blocked in 1% bovine serum albumin (BSA) in PBS for 1 h at room temperature. Upon washing thrice with PBS, the scaffolds were incubated in the diluted CD31 antibody (Abcam, USA) at 1:500 ratio, vinculin antibody (Abcam, USA) at 1:100 ratio, and VEGF antibody (Invitrogen, USA) at 1:200 ratio in 1% BSA overnight at 4°C. After washing thrice with PBS, the scaffolds were incubated with Alexa Fluor 488-conjugated goat anti-rabbit IgG H&L secondary antibody (1:500 dilution, Invitrogen, USA) in 1% BSA for 2 h at room temperature in the dark. In the following step, the scaffolds were stained with TRITC Phalloidin (Maokang Biotechnology, China) in 1% BSA for 30 min. The scaffolds were then stained with Hoechst 33342 (Solarbio Life Science, China) for 8 min after being washed with PBS thrice. The same protocol was used to stain the attached HUVECs on the outer surface of the P/G hydrogel scaffolds. Finally, the images of scaffolds were captured using a confocal microscope (TCS SP8 STED 3X, Leica, Germany).

2.8. Interaction of HUVECs with OCs

P/G₃ was chosen as the hydrogel concentration, and a 20-G needle was used. The wet spinning method was used to use sodium alginate as a tiny channel to communicate between endothelial cells and osteosarcoma cells. Cell viability of HUVECs and MG63 (Fuheng Biology, China) was first detected using Cell Counting Kit-8 (CCK-8) (Bimake, USA). The sterilized samples were washed three times with PBS, and 10 mL of Dulbecco's Modified Eagle Medium (DMEM; Gibco, Ireland) was added to the mixed hydrogel for 24 h to obtain the extracted solution of the hydrogel. Diluted 100 μL of the extracted solution containing 0%, 25%, 50%, 75%, and 100% of the mixed hydrogel was added to each well of a 96-well culture plate. Cell suspensions of HUVECs and MG63 were then added to the 96-well plates (5000 cells/well), respectively. Cell viability was detected using CCK-8 after 24 h and 48 h of incubation at 37°C in 5% CO₂. MG63 and HUVECs were injected into the channels according to the above method, immersed in DMEM medium, and cultured statically. The medium was changed daily and observed under a microscope (Olympus, Japan). After 5 days of culture, cytoskeletal and nuclear staining was performed on hydrogel scaffolds to study the interaction between OCs and HUVECs. Samples were washed with pre-warmed PBS and fixed with 4%

paraformaldehyde (BL539A, Biosharp, China) for 30 min at room temperature. Then, the samples were treated with 0.1% Triton X-100 (Triton X, Biosharp, China) diluted in PBS for 30 min. Subsequently, the samples were stained with TRITC Phalloidin (Maokang Biotechnology, China) in 1% BSA for 30 min. The samples were then stained with Hoechst 33342 (Solarbio Life Science, China) for 10 min and washed three times with PBS. Finally, images of the scaffolds were captured using a confocal microscope (TCS SP8 STED 3X, Leica, Germany).

2.9. *In vivo* study

This study was carried out following the recommendations of the Animal Care and Experiment Committee of Shanghai Ninth People's Hospital, Shanghai Jiao Tong University School of Medicine. The protocol was approved by the Animal Care and Experiment Committee of Shanghai Ninth People's Hospital, Shanghai Jiao Tong University School of Medicine (SH9H-2022-A11-1/SH9H-2022-A10-1). All methods were performed following relevant guidelines and regulations. A total of 12 eight-week-old male C57BL/6 mice were selected and randomly divided into four groups: the control group (no vascular scaffold), group I (1 × 1 scaffold), group II (4 × 4 scaffold), and group III (8 × 8 scaffold). Mice were anesthetized during surgery, and three mice in each group were implanted subcutaneously with hydrogel scaffold in the back. No signs of pain or discomfort were observed after surgery or throughout the study. The mice were kept in groups and monitored for 4 weeks. After 4 weeks of subcutaneous implantation, mice from each group were euthanized to remove the implanted scaffolds and surrounding tissues for initial observation of blood vessel formation in and around the implanted scaffolds. Samples were fixed with 4% paraformaldehyde solution for 48 h and paraffin-embedded. Sections (5 μm) were stained with hematoxylin and eosin (H&E) and Masson's trichrome, and the number of vessels was counted under a microscope. Sections were fluorescently double-stained (CD31, α-SMA) to examine the formation of vasculature^[35] and finally scanned. In addition, 24 six-week-old male Sprague-Dawley rats were selected and randomly divided into four groups: blank control group, group I (1×1 scaffold), group II (4×4 scaffold), and group III (8×8 scaffold). All rats were injected intraperitoneally with anesthetic, the inguinal skin of the left leg of the rat was incised, the artery was stripped out, and the proximal and distal points (distance about 8 mm) were ligated and cut off after ligation. The blank control group was injected with about 1 mL of PBS, while the hydrogel of the test group was implanted in the center of the ischemic vascular resection area of the rat after surgery, and the severed end of the vessel was placed above and to the side of the sample holder. The samples were fixed with sutures, and

the subcutaneous tissue and skin were sutured. Penicillin sodium was routinely administered intramuscularly for 3 consecutive days after surgery to prevent infection. Mice were housed and monitored in groups. The implanted stents and surrounding tissues were removed after 4 weeks and 8 weeks of *in vivo* implantation, respectively, for preliminary observation of blood vessel formation in and around the implanted stents. Samples were fixed in 4% paraformaldehyde solution for 48 h and then paraffin-embedded. Sections (5 μm) were stained with H&E and Masson's trichrome, and the number of vessels was counted under the microscope. The sections were stained with fluorescent double-labeling (CD31, α-SMA) and finally scanned.

2.10. Statistical analysis

Each experiment was performed in triplicate. The count data are presented as mean ± standard deviation. All quantitative data were analyzed using a one-way analysis of variance (ANOVA) with Tukey's significant difference *post-hoc* test for multiple comparisons (OriginPro 2021 Learning Edition, USA). Values of **p* < 0.05, ***p* < 0.01, and ****p* < 0.001 were considered statistically significant.

3. Results and discussion

3.1. Swelling compensation for 3D-printed vasculature

To investigate the potential of using the volume shrinkage induced by the P/G hydrogel to compensate for the swelling of the sacrificial template, a customized 3D printing platform based on an FDM printer and a syringe pump was used to print the sacrificial PF-127 (Figure 2A). Three needles of different sizes (19 G [I. D. 720 μm], 20 G [I. D. 610 μm], and 21 G [I. D. 520 μm]) (Figure 2B) were used to print the pre-designed zigzag path (Figure 2C). First, different feed rates of the sacrificial PF-127 were set to study their effect on the structure of printed sacrificial templates. In this section, the inner diameter of the needle was set as the designed diameter of the fiber in the printed sacrificial templates. As shown in Figure 2D, an ideal zigzag structure could be printed when the feed rate was set above 275 μL/min for a 19-G needle. The optimal feed rates for 20- and 21-G needles to obtain the target structure are 225 and 175 μL/min, respectively. Microscopy images of the printed sacrificial templates were captured, and the diameters of the template fibers were quantitatively analyzed, as shown in Figure 2E and F. Template fibers with a diameter of 750.6 ± 24.4 μm, which is close to the inner diameter of the 19-G needle, can be printed when the feed rate is set at 275 μL/min. For 20- and 21-G needles, the diameters of the template fibers were 638.4 ± 21.4 and 536.1 ± 33.7 μm, respectively, with feed rates set at 225

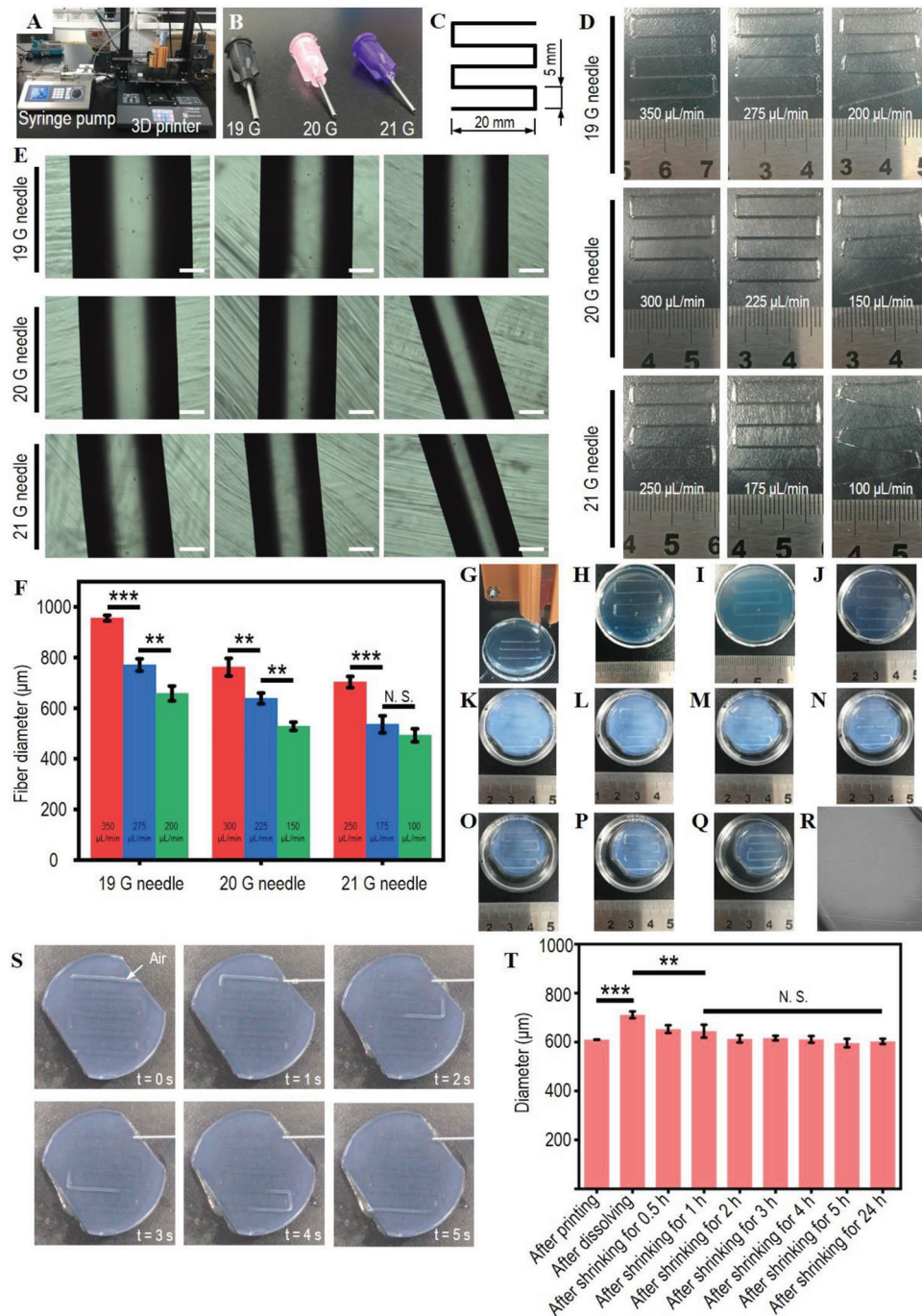


Figure 2. P/G hydrogel compensation for swelling of sacrificial template. (A) Customized 3D printing platform. (B) Needles of different sizes. (C) Designed zigzag printing path. (D) Printing of sacrificial PF-127 at different feed rates using various needles. (E) Microscopy images of the printed sacrificial PF-127 fiber at different feed rates using various needles. Scale bar = 200 μm. (F) Diameter of the sacrificial PF-127 fibers printed at different feed rates using various needles. (G) 3D printing of sacrificial PF-127 on a P/G hydrogel film. (H) Printed zigzag sacrificial template on P/G hydrogel film. (I) Encapsulation of sacrificial template in P/G hydrogel scaffold. (J) Removal of the sacrificial template. Shrinking of P/G hydrogel scaffold at (K) 0.5, (L) 1, (M) 2, (N) 3, (O) 4, (P) 5, and (Q) 24 h. (R) Magnified image of the fabricated vasculature after shrinking. (S) Injection of an air bubble into the vasculature after dissolving the sacrificial template. The black arrow denotes the injection direction. (T) Diameter of sacrificial PF-127 fiber and vasculature at different time points. n = 3 for each group.

and 175 $\mu\text{L}/\text{min}$. The results indicate that the sacrificial templates for the vasculature with the designed dimension could be printed by varying the feed rates of the sacrificial PF-127.

Then, the P/G_x hydrogel scaffolds with vasculature were prepared to observe the compensation phenomenon, where x represents the mass fraction of the GelMA in the P/G hydrogel. In this experiment, 1.5 mL freshly prepared P/G_3 hydrogel was crosslinked in a 35-mm Petri dish. Subsequently, the crosslinked hydrogel film was transferred to the 3D printing platform to print the sacrificial PF-127, as shown in Figure 2G. The 20-G needle was used in this printing process. The printed zigzag sacrificial template is shown in Figure 2H. Another 1.5 mL P/G_3 hydrogel was utilized to cover the printed sacrificial template (Figure 2I). The ends of the sacrificial templates were cut to facilitate the outflow of sacrificial PF-127, as shown in Figure 2J. After placing at 4°C for 20 min, ice-cold ultrapure water was gently injected into the channel to further clear the fabricated vasculature. The air was injected into the channel to verify the connectivity of the fabricated vasculature. The air bubbles flowed smoothly from one end of the vasculature to the other, verifying the successful preparation of the designed zigzag vasculature, as shown in Figure 2S. The FTIR spectra of PF-127 shows characteristic C-O-C stretching band at 1098 cm^{-1} , and C-H stretching band at 2880 cm^{-1} ^[36]. As shown in Figure S1 (Supplementary File), the P/G hydrogel after the sacrificial template is removed does not contain the characteristic peak of PF-127, so the sacrificial template was completely removed. Finally, the hydrogel scaffold with the 35-mm Petri dish was floated in a 37°C water bath to observe the shrinking process. Images of the hydrogel scaffold with vasculature were captured at 0.5, 1, 2, 3, 4, 5, and 24 h and are shown in Figure 2K–Q, respectively. The vasculature was still noticeable after the volume shrinkage (Figure 2R).

The diameters of the prepared vasculature before and after shrinking were recorded in Figure 2T. After printing, the diameter of the fiber in the sacrificial template was $609.8 \pm 0.7\ \mu\text{m}$, which is close to the inner diameter of the 20-G needle (I. D. $610\ \mu\text{m}$). However, after dissolving, the diameter of the prepared vasculature increased to $711.4 \pm 13.8\ \mu\text{m}$. After shrinking at 37°C for 2 h, the diameter of the vasculature was maintained at around $610\ \mu\text{m}$. The results indicate that although the vasculature with a designed diameter can be fabricated by switching the feed rate of the sacrificial PF-127, the swelling of the sacrificial template during the dissolution process still leads to the deformation of the vasculature size. However, the volume shrinkage of the thermosensitive P/G hydrogel can compensate for the swelling of the sacrificial template,

which shows great potential for the precise fabrication of engineered vasculature.

3.2. Effect of PNIPAM/GelMA (P/G) concentration on swelling compensation

The concentration of P/G hydrogel determines its volume shrinkage degree. Thus, the effect of P/G hydrogel concentration on the swelling compensation was studied in this section. Different concentrations of GelMA were mixed with PNIPAM to form P/G_1 , P/G_3 , and P/G_5 hydrogels. NIPAM, MBA, and LAP concentrations were fixed at 10, 0.15, and 0.075 wt%, respectively. A 20-G needle was used in this section. Images of the P/G hydrogel scaffolds before and after shrinking at 37°C were captured (Figure 3A). The diameter of the prepared vasculature during this process and the shrinkage ratio of the P/G hydrogel scaffolds were analyzed, as shown in Figure 3B and C, respectively. The results demonstrated that all scaffolds showed significant shrinkage within the first 2 h at 37°C . Subsequently, the shrinking process of the P/G hydrogel scaffolds slowed down, which was consistent with the results in section 3.1. The diameter of the fabricated vasculature increased with the increase of GelMA concentration, and only the diameter of vasculature in P/G_3 hydrogel scaffolds was maintained around the designed size, as shown in Figure 3B. This is mainly attributed to the dense crosslinked network in GelMA with high concentration. The dense crosslinked network impedes the water release in the P/G hydrogel at 37°C , which further hinders the volume shrinkage of the P/G hydrogel. This is also demonstrated by the shrinkage ratio of P/G hydrogel constructs. Specifically, the volume shrinkage degree of the P/G hydrogel scaffold gradually decreased with the increase of GelMA concentration, as shown in Figure 3C.

The contact angle of P/G_1 , P/G_3 , and P/G_5 hydrogel scaffolds at 25°C and 37°C was measured to explore the surface characteristics. As shown in Figure S2 (Supplementary File), the contact angles of all the P/G hydrogel scaffolds were maintained at around 20° . The contact angle of P/G_1 , P/G_3 , and P/G_5 hydrogel constructs increased to $67.4 \pm 8.0^\circ$, $42.2 \pm 1.3^\circ$, and $29.5 \pm 3.8^\circ$ after increasing the temperature to 37°C . The increase of GelMA concentration denotes the decrease in the concentration ratio of PNIPAM and GelMA. The volume shrinkage of P/G hydrogel is caused by the hydrophilicity and hydrophobicity switch of PNIPAM below and above the LCST, respectively, at around 32°C . Below the LCST, the PNIPAM hydrogel is hydrophilic. When above the LCST, PNIPAM becomes hydrophobic^[37,38]. Thus, the decrease in the P/G concentration ratio reduces the shrinkage ability of the hydrogel. This further shows that the high concentration of GelMA can negatively affect the volume shrinkage ratio.

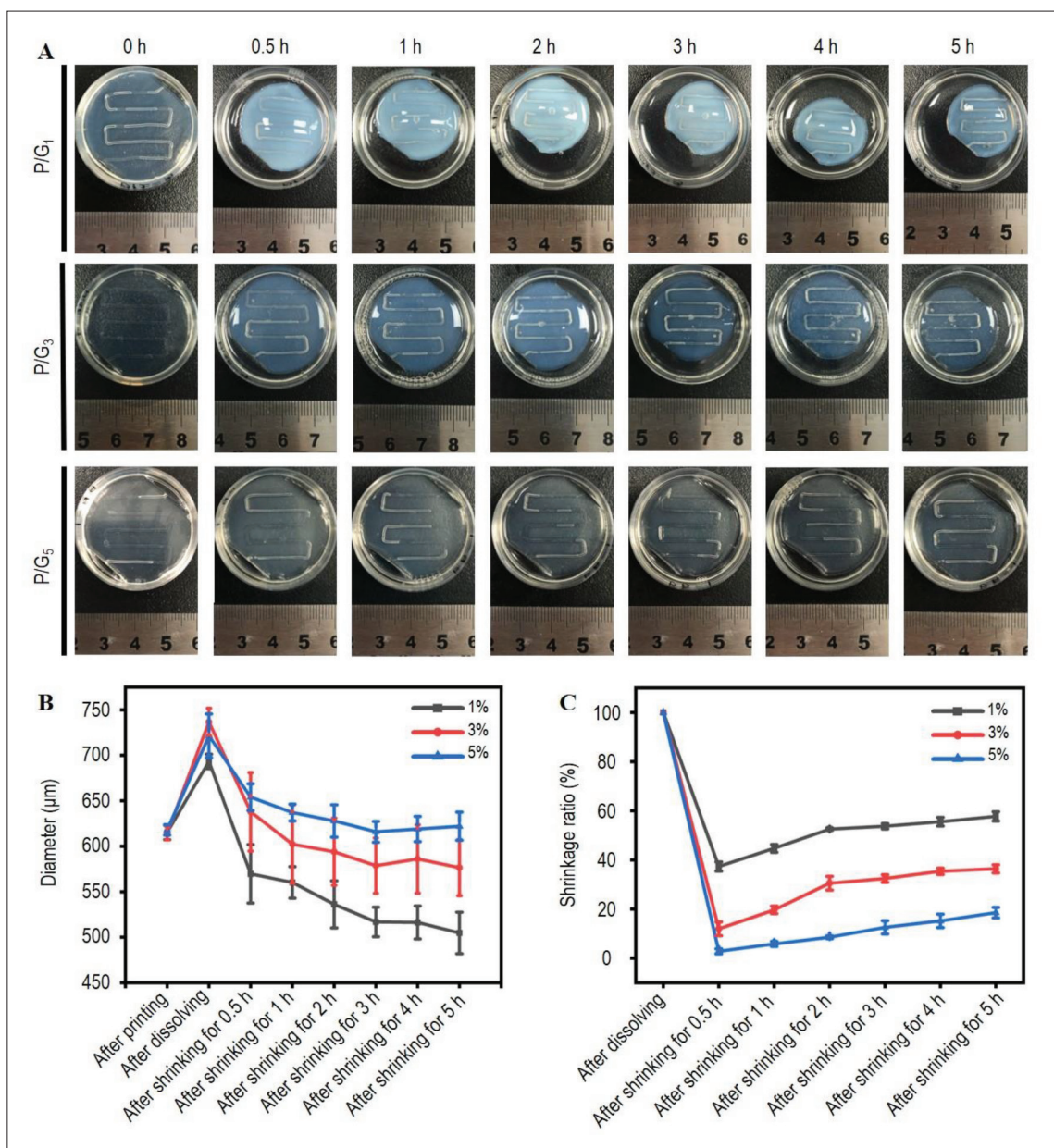


Figure 3. Effect of P/G concentration on swelling compensation. (A) Images of hydrogel scaffolds with vasculature prepared with different P/G concentrations at various shrinking time points. (B) Diameter of printed sacrificial PF-127 fibers and vasculature at different time points. (C) Shrinkage ratio of hydrogel scaffolds with vasculature prepared with different P/G concentrations. n = 3 for each group.

3.3. Effect of vasculature density on the swelling compensation

The vasculature increases the surface area for the P/G hydrogel scaffold with the air, which provides a channel for the water to be released from the hydrogel when placed at 37°C. Thus, the effect of vasculature density on the swelling compensation was explored in this section. Three patterns with three, six, and nine fibers of vasculature in Figure 4A were designed. P/G₂, P/G₃, and P/G₄ were used in this section. A 20-G needle was used for the printing

of sacrificial PF-127. After complete crosslinking, the sacrificial template was removed, and the P/G hydrogel scaffold with the 35-mm Petri dish was floated in the water bath at 37°C to observe the shrinking process. Red acrylic paint was injected into the vasculature to distinguish various densities.

The images of P/G₃ hydrogel scaffolds during the shrinking process were captured, as shown in Figure 4B. Images of P/G₂ and P/G₄ hydrogel scaffolds are displayed

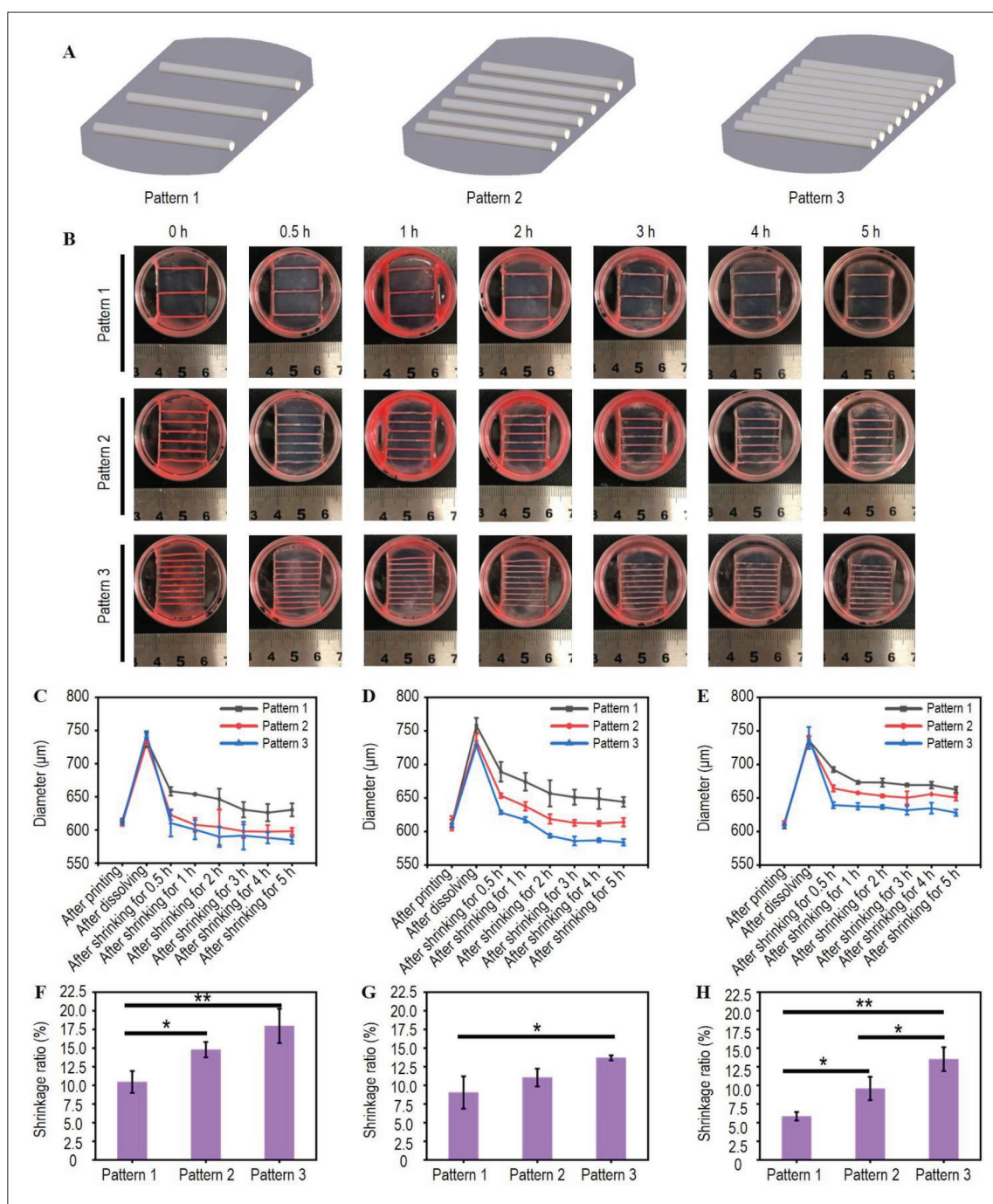


Figure 4. Vasculature density effect on swelling compensation. (A) Designed vasculature patterns with different densities. (B) Images of P/G₃ hydrogel constructs with different vasculature densities at different shrinking time points. (C, D, and E) Diameter of printed sacrificial F-127 fibers and vasculature at different shrinking time points for P/G₂, P/G₃, and P/G₄ hydrogel constructs, respectively. (F, G, and H) Shrinkage ratio of P/G₂, P/G₃, and P/G₄ hydrogel scaffolds with different vasculature densities, respectively. n = 3 for each group.

in **Figures S3 and S4** (Supplementary File). The diameter of the fibers in sacrificial templates and the vasculature in P/G₂, P/G₃, and P/G₄ hydrogel scaffolds before and after shrinking were recorded in **Figure 4C–E**, respectively. The shrinkage ratio of P/G₂, P/G₃, and P/G₄ hydrogel

scaffolds was computed and is shown in **Figure 4F–H**, respectively. The results showed that the vasculature with different densities has the same trend of swelling and volume shrinkage behaviors. Specifically, the diameter of the vasculature after shrinking for 2 h decreased upon

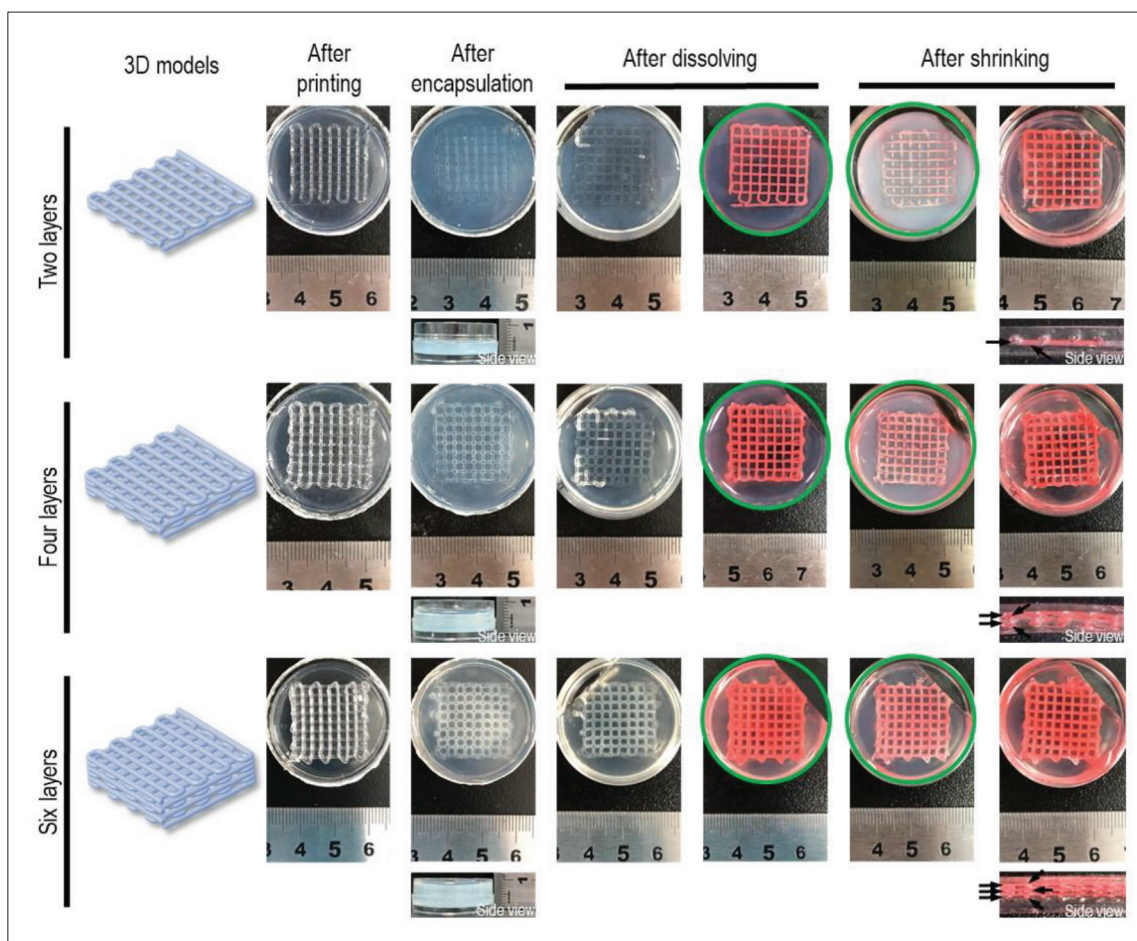


Figure 5. Fabrication of 3D vasculature within the P/G hydrogel scaffolds by printing sacrificial templates with multiple layers.

increasing the vasculature density. For P/G_2 hydrogel constructs, the diameter of vasculature was maintained at $\sim 600 \mu\text{m}$ for Patterns 2 and 3, while the diameter of vasculature in Pattern 1 increased to $646.4 \pm 15.9 \mu\text{m}$. For P/G_3 hydrogel constructs, the diameter of vasculature in Pattern 2 was similar to the designed size. The diameters of vasculature in Patterns 1 and 3 were 656.9 ± 19.5 and $593.6 \pm 2.8 \mu\text{m}$, respectively. For P/G_4 hydrogel constructs, the diameters of vasculature for all patterns were above $630 \mu\text{m}$. This may be caused by the high surface area of high-density vasculature that can facilitate the outflow of the water in P/G hydrogel scaffolds. Thus, the size of the engineered vasculature can be tuned by adjusting the P/G concentration and vasculature density.

3.4. Fabrication of 3D vasculature

In Figure 1, the sacrificial template was printed on the P/G hydrogel film, exhibiting a two-dimensional vasculature. To investigate the potential of our method to fabricate 3D vasculature, sacrificial templates with multiple layers were designed and printed on the P/G hydrogel film, as

shown in Figure 5. P/G_3 hydrogel and a 20-G needle were used in this experiment. The images of the P/G hydrogel scaffolds at different time points were captured, and the red acrylic paint was injected into the vasculature to verify its 3D structure. The top and side view images of the P/G hydrogel scaffolds indicate the connectivity of the fabricated vasculature before and after shrinking. Volume shrinkage of P/G hydrogel scaffolds with two and four layers of the vasculature at 37°C was observed, while no significant shrinkage was found for the P/G hydrogel scaffold with six layers of vasculature. This is mainly due to the large volume of P/G hydrogel to encapsulate the sacrificial template with six layers, which makes it difficult for the water inside the P/G hydrogel to be released. However, the P/G hydrogel scaffolds with six layers of vasculature considerably shrunk at 37°C when P/G_1 and P/G_2 hydrogels were applied, as shown in Figure S5 (Supplementary File). Thus, we can further confirm that the volume shrinkage degree of the P/G hydrogel scaffold can be tuned by changing the hydrogel concentration, vasculature density, and vasculature structure to fabricate

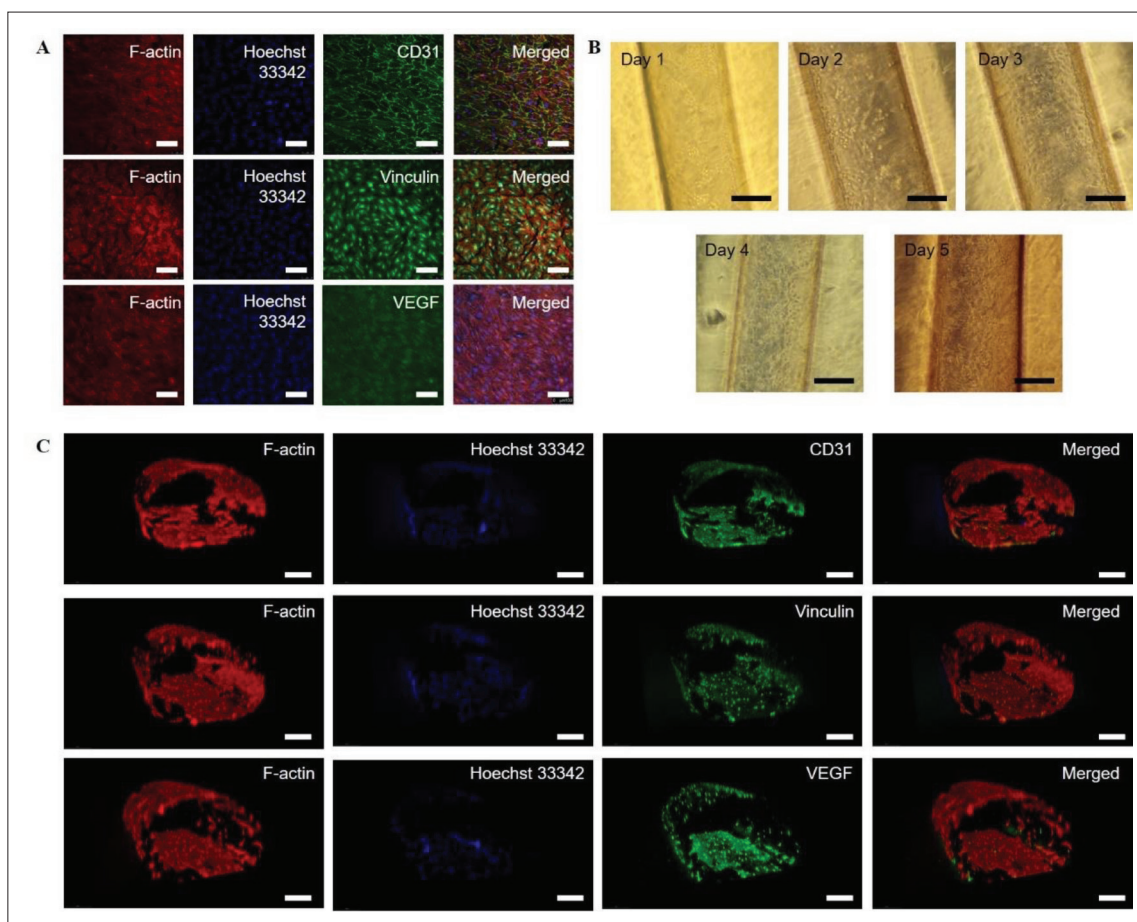


Figure 6. Formation of endothelial layer in the vasculature lumen with P/G hydrogel scaffolds. (A) Immunofluorescence staining of CD31, vinculin, and VEGF of HUVECs attached to the surface of P/G hydrogel scaffolds. Scale bar = 100 μm . (B) Microscopy image of HUVECs attached to the inner surface of the vasculature lumens during culturing. Scale bar = 200 μm . (C) Immunofluorescence staining of CD31, vinculin, and VEGF of HUVECs attached to the inner surface of the vasculature lumen after culturing for 5 days. Scale bar = 200 μm .

vasculature of the designed size. It is also possible to prepare vascular scaffolds with curved structures as shown in [Figure S6](#) (Supplementary File), which demonstrates the printing method can be used to fabricate vasculature with complicated structure.

3.5. Formation of endothelial monolayer

Although both PNIPAM and GelMA are widely used hydrogels in tissue engineering and cell culture matrixes owing to their biocompatibility, the cell viability of the P/G hydrogel and the formation of endothelial monolayer within the vasculature fabricated by the proposed method remain unknown. HUVECs were cultured on the surface of the P/G₃ hydrogel to investigate the attachment of cells. After culturing for 5 days, immunofluorescence staining of CD31, vinculin, and VEGF was performed on the P/G₃ hydrogel to evaluate the cell viability ([Figure 6A](#)). The expression of CD31, vinculin, and VEGF indicates that the HUVECs maintained high viability on the P/G₃

hydrogel, suggesting that the P/G hydrogel preserves biocompatibility for cells.

We first used PF-127 as the sacrificial material to fabricate vasculature for the formation of an endothelial monolayer on its inner surface. The 20-G needle and Pattern 2 structure in [Figure 4](#) were used in this section. The HUVECs' suspension was injected into the lumen of the engineered vasculature within the P/G₃ hydrogel scaffolds to assess the formation of the endothelial monolayer. Although the cells could attach to the inner surface of the vasculature during the first 3 days of culture, no evident proliferation of cells was observed, as shown in [Figure S7](#) (Supplementary File). Moreover, most cells lost their spindle-like morphologies after culturing for 3 days, which means that the cells tend to detach from the inner surface of the vasculature. During the printing of F-127, the smooth surface of F-127 could be observed^[39]. Thus, the detachment of cells may be attributed to the smooth

surface of the vasculature after removing the sacrificial PF-127. SEM images of the vasculature surface showed that the vasculature fabricated by PF-127 was glossy (Figure S8 in Supplementary File), which may make it difficult for cells to attach to and grow on. Thus, in this experiment, 5% (w/v) gelatin was added to PF-127 to change the morphology of the vasculature surface, as gelatin exhibits a granular structure in the sacrificial PF-127 hydrogel. SEM images of the vasculature fabricated by PF-127 + gelatin showed that the vasculature surface has a honeycomb structure packed with grooves (Figure S8 in Supplementary File). Cells tend to adhere to a rough surface more than to a smooth one^[40]. Thus, the porous structure can benefit the attachment of cells. As shown in Figure S7 (Supplementary File), the cells could stably attach to the vasculature surface with spindle-like morphologies during the culturing. Significant cell proliferation was discerned. Thus, PF-127 + gelatin was selected as the sacrificial material in this experiment.

For the formation of the endothelial monolayer, the growth of HUVECs inside the lumens was recorded every day (Figure 6B). The results showed that the HUVECs could distribute on the surface of the vasculature lumens and predominately form spindle-like morphologies, which further indicates the biocompatibility of the P/G hydrogel. The number of cells significantly increased during the culturing. After 5 days of culturing, the HUVEC monolayer could be visualized in the microscopy images. Immunofluorescence staining of CD31, vinculin, and VEGF of the formed endothelial monolayer was conducted on day 5 to evaluate the endothelialization of the HUVECs attached to the inner surface of the vasculature lumen. As shown in Figure 6C, cells were interconnected and formed the endothelial monolayer in the inner surface of the vasculature lumen. High expression of the CD31 marker demonstrated the attainment of endothelial function. As a pivotal protein marker in the cell–scaffolds interaction, the appearance of the vinculin maker suggests that the firm adhesion of the HUVECs was achieved on the inner surface of the vasculature lumen. Moreover, the enormous expression of VEGF for angiogenesis further exhibits the potential of the P/G hydrogel scaffolds with vasculature to support vascularization. Although PNIPAM has been reported to be cytotoxic to endothelial cells^[41], we prepared a hydrogel scaffold by mixing GelMA with PNIPAM to enhance the cell adhesion of P/G hydrogel since GelMA has been widely used as a good cytocompatible material^[42–44]. From the above results, it can be seen that P/G hydrogels have good cytocompatibility and good expression of relevant markers.

3.6. Interaction between HUVECs and OCs

In this section, the engineered vasculature was utilized as an *in vitro* model to explore the interaction between HUVECs

and OCs. P/G₃ hydrogel was prepared as described previously. The prepared hydrogel extracts were added to the cell culture medium at different concentrations (0%, 25%, 50%, 75%, and 100%) and incubated with HUVECs and MG63 for 24 and 48 h, respectively. After 24 and 48 h of incubation, the cell survival rate of each group was found to be not significantly different after assaying with the CCK-8 test (Figure S9 in Supplementary File), indicating that the P/G hydrogel extracts were non-toxic to the cells. For the micro-channel, sodium alginate sacrificial fibers were wet-spun in calcium chloride solution and orderly arranged on the crosslinked P/G₃ hydrogel, as shown in Figure 7A. 34-G (I. D. 60 μm , O. D. 230 μm) needle was used in this study. After that, PF-127 + gelatin sacrificial fibers were printed on the sodium alginate sacrificial fibers and the crosslinked P/G₃ hydrogel to serve as macro-channel and cellular channel. PF-127 + gelatin and sodium alginate were removed in ethylenediaminetetraacetic acid disodium salt (EDTA-2Na) at 4°C after crosslinking by light. Subsequently, the hierarchical vasculature model shrunk at 37°C for 2 h to prepare an *in vitro* model for HUVECs and OCs, as shown in Figure 7A. MG63 and HUVECs were injected into the prepared *in vitro* model shown in Figure 7B, and the growth status of both cells was observed.

The results revealed that OCs could migrate into the micro-channels after culturing with HUVECs. It could be seen on confocal fluorescence imaging that MG63 and HUVECs in the experimental group spread throughout the channels, as shown in Figure 8. The enlarged views of HUVECs and OCs in the experimental group can be seen from Figure S10A (Supplementary File). In the control group, OCs could not migrate into the micro-channels and grew in a single channel when culturing without HUVECs, as shown in Figure 8 as well as Figure S10B and S10C (Supplementary File). However, HUVECs could migrate to other channels along the micro-channels when culturing without OCs, confirming that this engineered vasculature model has good biocompatibility and can promote the growth of endothelial cells to promote blood vessel formation. Thus, the engineered vasculature within the P/G hydrogel fabricated in this study can be a potential model for drug screening and organ-on-a-chip.

3.7. *In vivo* study

To evaluate the *in vivo* vessel formation ability of the P/G hydrogel, scaffolds with vasculature, scaffolds without vasculatures for the control group, and scaffolds (1 \times 1, 4 \times 4, and 8 \times 8) with a different number of vasculatures were implanted subcutaneously in mice. The size of the scaffolds in each group was 1 \times 1 \times 0.2 cm. The P/G₃ hydrogel and 20-G needle were used in this experiment. After 4 weeks of implantation, the scaffolds with the surrounding skin were

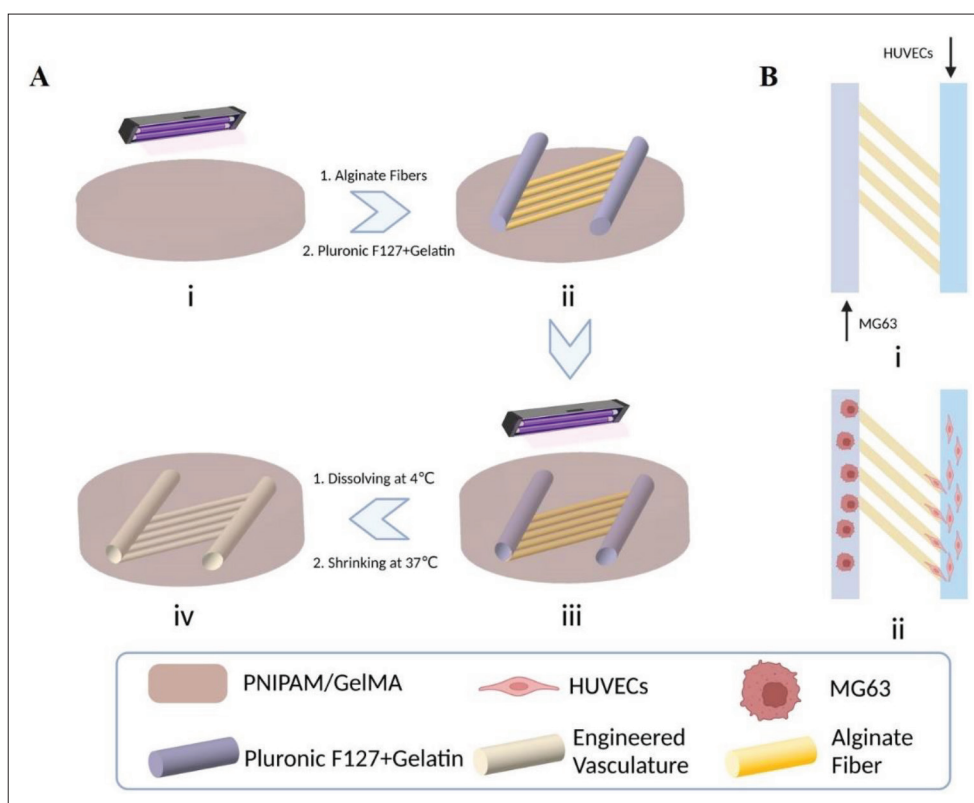


Figure 7. Schematic diagram of the preparation of *in vitro* model with hierarchical vasculature for studying the interaction between HUVECs and OCs. Created with BioRender.com.

extracted from the sacrificed mice. First, no inflammation or abnormalities were found in the surrounding tissues in all the groups after 4 weeks of implantation, indicating the good biocompatibility of the P/G hydrogel scaffolds. More blood vessels were observed around the scaffolds with vasculature compared with the control group's scaffolds. Blood was observed in the vasculature within the 1×1 , 4×4 , and 8×8 scaffolds in the gross observation images, as shown in Figure 9A. The number of vascular branches and the vascular length around the scaffolds were calculated (Figure S11 in Supplementary File). The number of branches around the 4×4 and 8×8 scaffolds was 18 ± 1.0 and 24 ± 7.8 , respectively, which was considerably higher than the number of branches found around the control group's scaffold and 1×1 scaffold (Figure S11A in Supplementary File). The vascular length around the scaffolds increased with the increase in vascular density (Figure S11B in Supplementary File). The results demonstrated that the scaffolds with engineered vasculature can promote the blood vessel infiltration and growth of neighboring host vessels in the surrounding tissues. This is mainly due to the mass transport function of the fabricated vasculature within the P/G hydrogel scaffolds. To demonstrate that the host vessels can grow into the prepared vasculature, the scaffolds used for animal

experiments were prepared without cells. However, the host vessels within the engineered vasculature, which have a great potential for anastomosis, will be a focus for further study.

H&E and Masson's trichrome staining images are displayed in Figure 9B and C. No new tissues or red blood cells were formed in the center of the control group's scaffolds. In the scaffolds with vasculature, all hollow channels of the vasculature were fully filled with new tissue after the implantation. Magnified images of the vasculature lumens within 1×1 , 4×4 , and 8×8 scaffolds are displayed in Figure 9E(i)–(iii), respectively. Red blood cells were visible within the vasculature lumens. Immunofluorescence staining of CD31 and α -SMA was conducted to further confirm the formation of vessels in the engineered vasculature (Figure 9D). Magnified images of the vasculature lumens within 1×1 , 4×4 , and 8×8 scaffolds are displayed in Figure 9F(i)–(iii), respectively. Vascular structures were found to be densely distributed in the 8×8 scaffold group (Figure 9F(iii)). Although the expression of α -SMA could be detected in the vasculature lumens within the 1×1 and 4×4 scaffolds, no complete circular structure of α -SMA was observed (Figure 9F(i) and (ii)). The results suggest that the engineered

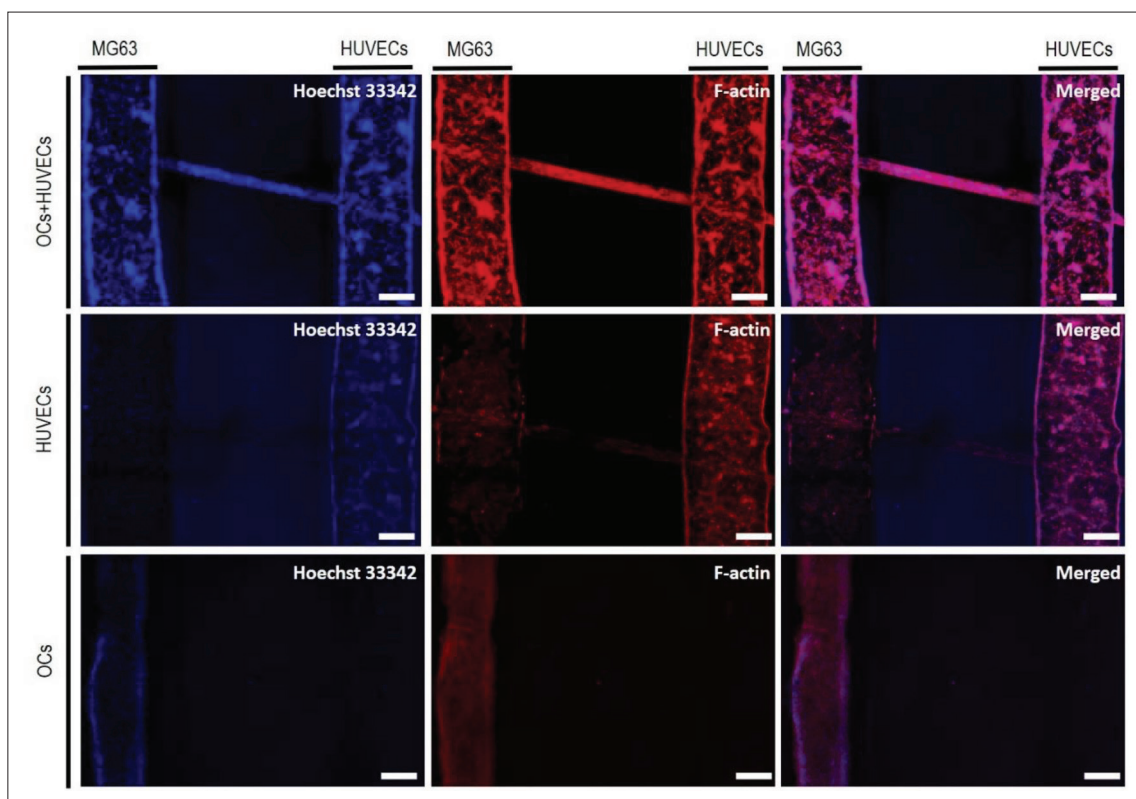


Figure 8. Interaction of HUVECs with OCs in engineered vasculature. Scale bar = 100 μ m.

vasculature is beneficial for blood perfusion and tissue formation. Among the other groups, no tissue growth was observed for the scaffolds without vasculature. Meanwhile, the vascular formation was significantly better in the vasculature lumens within 8×8 scaffolds, revealing that the high density of vasculature played a crucial role in tissue growth and vascular formation. In addition, **Figure S11C** (Supplementary File) shows the compressive stress–strain curves for the control group (no vascular scaffold), group I (1×1 scaffold), group II (4×4 scaffold), and group III (8×8 scaffold). With the increase of vasculature density, the compression modulus decreases. This is mainly due to the high density of vasculature channels that cannot support the pressure.

In addition, in order to further evaluate the blood vessel infiltration of the developed engineered vasculature, we implanted the engineered vasculature into a rat hindlimb ischemia model, as shown in **Figure S13A** (Supplementary File). The same scaffolds as that implanted subcutaneously in mice were used in this section. After severing the blood vessels in the left leg of the rat, it was observed that the left sole of the rat was white, while the skin color of the right sole was normal, indicating that the ischemia model was successfully constructed (**Figure S13B** in Supplementary File). No abnormalities were observed after implantation

of the engineered vascular scaffold. The scaffold and surrounding tissues were removed from the hind limbs of sacrificed rats 4 and 8 weeks after implantation, respectively. The H&E and Masson's trichrome staining results showed that the hydrogel scaffold with blood vessels implanted in the rats could promote blood vessel growth compared with the control group, as shown in **Figure 10**. The ability of blood vessel infiltration increased with the increase of the engineered vasculature density. The fluorescence images showed that the α -SMA expression increased with the increase of the engineered vasculature density. There was a higher α -SMA expression at the 8th week, which demonstrated better connection of the engineered vasculature with the surrounding tissues (**Figures S12, S13C, and S13D** in Supplementary File). Thus, the results showed that the engineered vasculature could support the blood vessel infiltration even in the ischemic environment, which further accentuated the importance of the engineered vasculature.

4. Conclusion

We report a small method induced by volume shrinkage to compensate for the swelling caused by sacrificial materials used in 3D printing to precisely fabricate engineered vasculature within thermoresponsive P/G

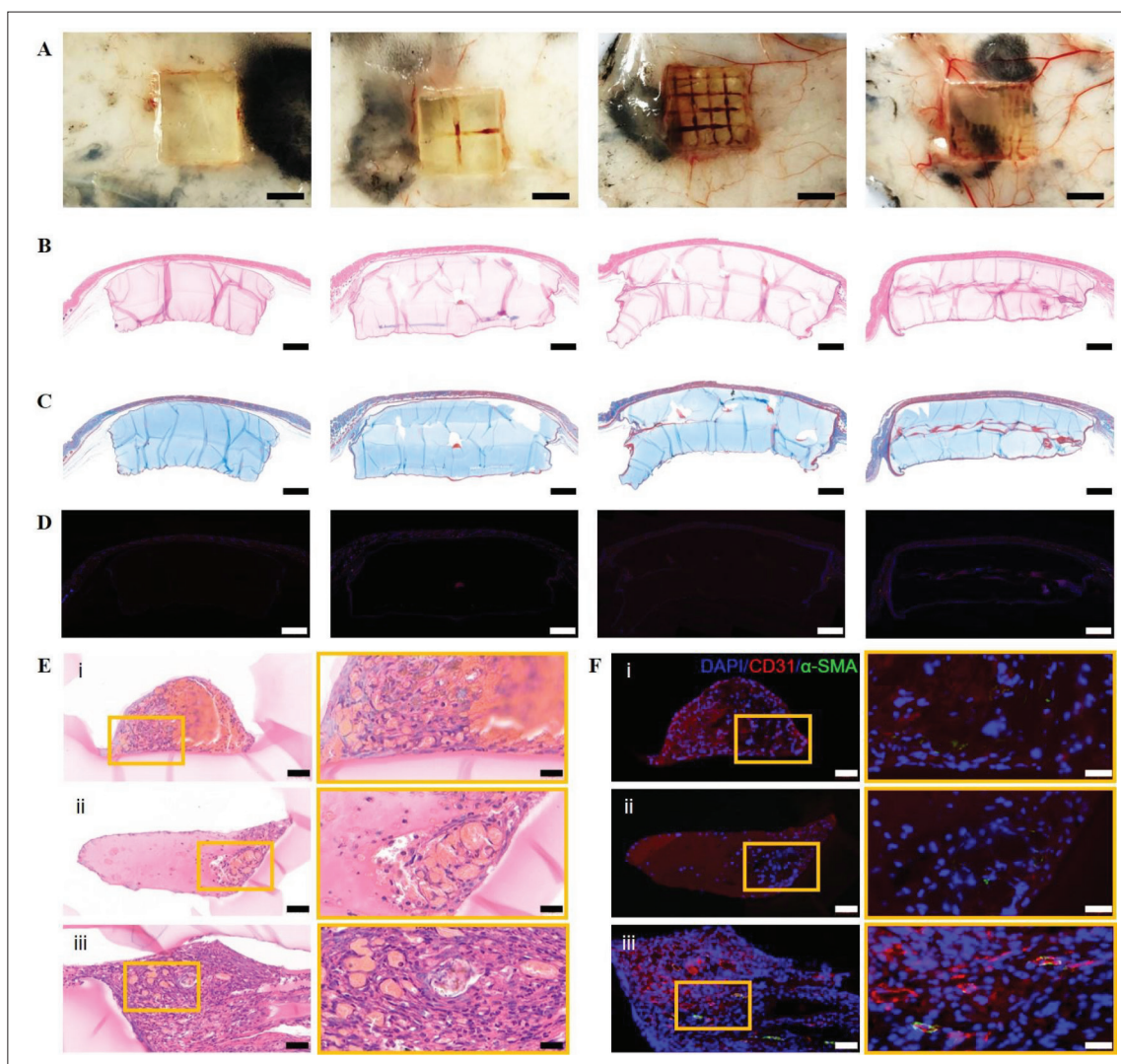


Figure 9. Subcutaneous implantation of scaffolds with engineered vasculature. (A) Gross observation images of P/G hydrogel scaffolds after subcutaneous implantation for 4 weeks in C57BL/6 mice. Scale bar = 500 μm . (B) H&E staining for the implanted scaffolds and surrounding tissues. Scale bar = 1 mm. (C) Masson's trichrome staining for the implanted scaffolds and surrounding tissues. Scale bar = 1 mm. (D) Immunofluorescence staining of CD31 and α -SMA for the implanted scaffolds and surrounding tissues. Scale bar = 1 mm. (E) H&E staining of the vasculature lumens within the (i) 1×1 , (ii) 4×4 , and (iii) 8×8 scaffolds. Scale bar = 50 μm ; scale bar in the magnified images = 20 μm . (F) Immunofluorescence staining of CD31 and α -SMA for the vasculature lumens within the (i) 1×1 , (ii) 4×4 , and (iii) 8×8 scaffolds. Scale bar = 50 μm ; scale bar in the magnified images = 20 μm .

hydrogel. The P/G hydrogel exhibited volume shrinkage at 37°C . Engineered vasculature with a designed diameter can be accurately fabricated by tuning the concentration ratio of PNIPAM and GelMA. The density of vasculature can also be altered to fabricate vasculature of an ideal size. The proposed method is able to fabricate vasculature with 3D structures. *In vitro* and *in vivo* results demonstrated that the prepared P/G hydrogel scaffolds exhibit good biocompatibility and capability to promote blood vessel growth in products made by engineered regeneration and biomanufacturing. These results show that our proposed method holds great potential in the

precise fabrication of vasculature, and the fabricated vasculature could facilitate blood vessel infiltration into the vasculature of the P/G hydrogel scaffolds for tissue engineering applications.

Acknowledgments

None.

Funding

This study was supported by funds from the National Key R&D Program of China (2018YFA0703000), Projects

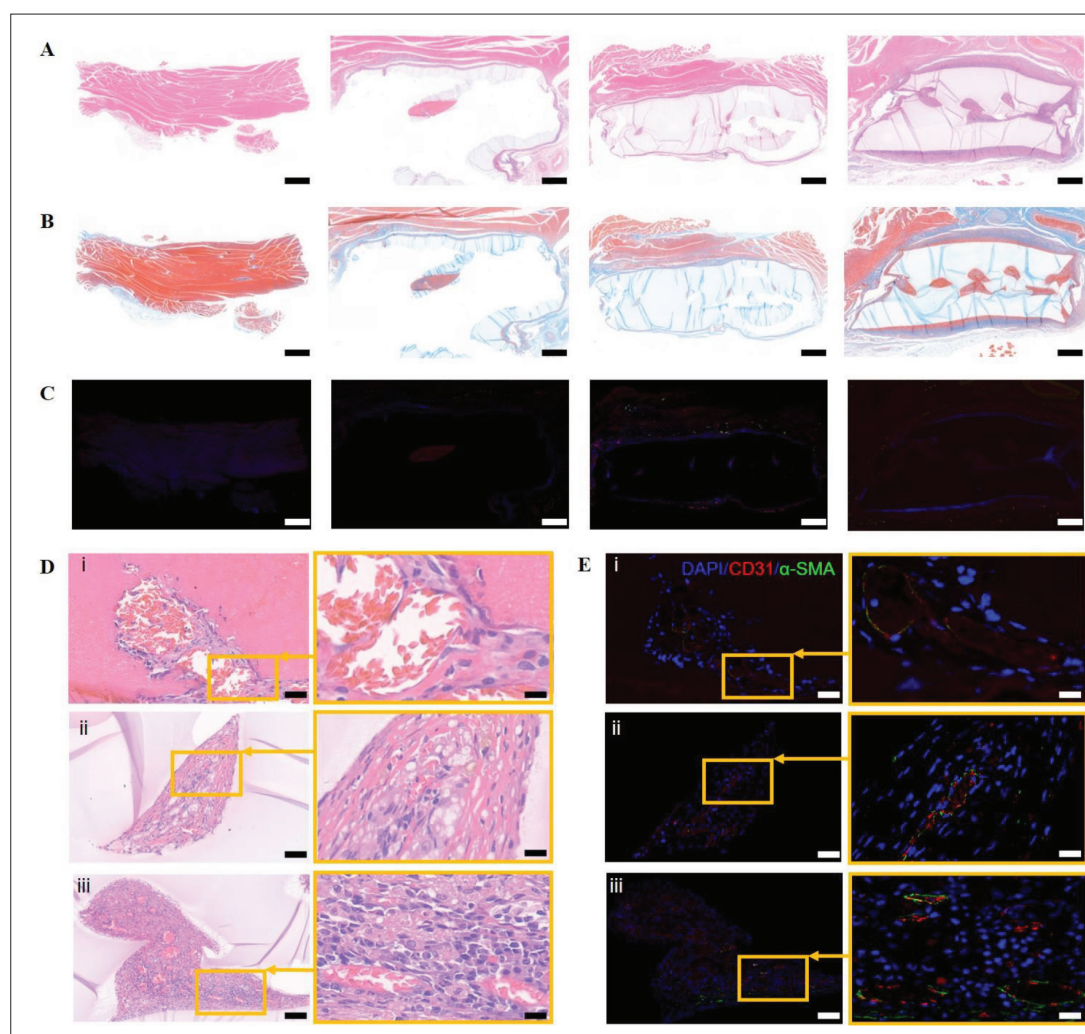


Figure 10. Implantation of scaffolds with engineered vasculature in ischemia model for 4 weeks. (A) H&E staining for the implanted scaffolds and surrounding tissues. Scale bar = 1 mm. (B) Masson's trichrome staining for the implanted scaffolds and surrounding tissues. Scale bar = 1 mm. (C) Immunofluorescence staining of CD31 and α -SMA for the implanted scaffolds and surrounding tissues. Scale bar = 1 mm. (D) H&E staining of the vasculature lumens within the (i) 1×1 , (ii) 4×4 , and (iii) 8×8 scaffolds. Scale bar = 50 μ m; scale bar in the magnified images = 20 μ m. (E) Immunofluorescence staining of CD31 and α -SMA for the vasculature lumens within the (i) 1×1 , (ii) 4×4 , and (iii) 8×8 scaffolds. Scale bar = 50 μ m; scale bar in the magnified images = 20 μ m.

funded by the China Postdoctoral Science Foundation (2020TQ0195/2021M702165/2022M722121), the National Natural Science Foundation of China (NSFC) Research Grants (82072412/81772326/81902195), Postdoctoral Incentive Program of Shanghai Jiao Tong University School of Medicine, Project of Shanghai Science and Technology Commission (19XD1434200), Two-hundred Talent Support (20152224), Translational Medicine National Key Science and Technology Infrastructure (Shanghai) Open Project (TMSK-2020-118), and Translational Medicine Innovation Project of Shanghai Jiao Tong University School of Medicine (TM201613).

Conflict of interest

The authors declare no conflict of interest.

Author contributions

Conceptualization: Xue Yang, Shuai Li, Jinwu Wang, Kerong Dai

Formal analysis: Xue Yang, Shuai Li

Investigation: Xue Yang, Xin Sun, Lei Qiang, Yihao Liu

Methodology: Xin Sun, Ya Ren

Resources: Jinwu Wang, Kerong Dai

Supervision: Shuai Li, Jinwu Wang, Kerong Dai

Writing – original draft: Xue Yang, Shuai Li

Writing – review & editing: Xue Yang, Shuai Li, Xin Sun, Ya Ren

Ethics approval and consent to participate

This study was carried out following the recommendations of the Animal Care and Experiment Committee of Shanghai Ninth People's Hospital, Shanghai Jiao Tong University School of Medicine. The protocol was approved by the Animal Care and Experiment Committee of Shanghai Ninth People's Hospital, Shanghai Jiao Tong University School of Medicine (SH9H-2022-A11-1/SH9H-2022-A10-1).

Consent for publication

Not applicable.

Availability of data

The data that support the findings of this study are available upon reasonable request from the authors.

References

1. Dumas SJ, Meta E, Borri M, *et al.*, 2021, Phenotypic diversity and metabolic specialization of renal endothelial cells. *Nat Rev Nephrol*, 17(7): 441–464.
<https://doi.org/10.1038/s41581-021-00411-9>.
2. Liu X, Wang X, Zhang L, *et al.*, 2021, 3D liver tissue model with branched vascular networks by multimaterial bioprinting. *Adv Healthc Mater*, 10(23): 2101405.
<https://doi.org/10.1002/adhm.202101405>.
3. Zhu Y, Kong B, Liu R, *et al.*, 2022, Developing biomedical engineering technologies for reproductive medicine. *Smart Med*, 1(1): e20220006.
<https://doi.org/10.1002/smmd.20220006>.
4. Fu Z, Zhuang Y, Cui J, *et al.*, 2022, Development and challenges of cells- and materials-based tooth regeneration. *Eng Reg*, 3(2): 163–181.
<https://doi.org/10.1016/j.engreg.2022.04.003>.
5. Gao Y, Ma Q, 2022, Bacterial infection microenvironment-responsive porous microspheres by microfluidics for promoting anti-infective therapy. *Smart Med*, 1(1): e2022001.
<https://doi.org/10.1002/smmd.20220012>.
6. Sarker MD, Naghieh S, Sharma NK, *et al.*, 2018, 3D biofabrication of vascular networks for tissue regeneration: a report on recent advances. *J Pharm Anal*, 8(5): 277–296.
<https://doi.org/10.1016/j.jpha.2018.08.005>.
7. Nie J, Gao Q, Wang Y, *et al.*, 2018, Vessel-on-a-chip with hydrogel-based microfluidics. *Small*, 14(45): 1802368.
<https://doi.org/10.1002/sml.201802368>.
8. John JV, McCarthy A, Wang H, *et al.*, 2021, Freeze-casting with 3D-printed templates creates anisotropic microchannels and patterned macrochannels within biomimetic nanofiber aerogels for rapid cellular infiltration. *Adv Healthc Mater*, 10(12): 2100238.
<https://doi.org/10.1002/adhm.202100238>.
9. Zhang B, Radisic M, 2020, Organ-level vascularization: The Mars mission of bioengineering. *J Thorac Cardiovasc Surg*, 159(5): 2003–2007.
<https://doi.org/10.1016/j.jtcvs.2019.08.128>.
10. Kinstlinger IS, Saxton SH, Calderon GA, *et al.*, 2020, Generation of model tissues with dendritic vascular networks via sacrificial laser-sintered carbohydrate templates. *Nat Biomed Eng*, 4(9): 916–932.
<https://doi.org/10.1038/s41551-020-0566-1>.
11. Cui H, Esworthy T, Zhou X, *et al.*, 2020, Engineering a novel 3D printed vascularized tissue model for investigating breast cancer metastasis to bone. *Adv Healthc Mater*, 9(15): 1900924.
<https://doi.org/10.1002/adhm.201900924>.
12. Lee B, Kim S, Ko J, *et al.*, 2022, 3D micromesh-based hybrid bioprinting: Multidimensional liquid patterning for 3D microtissue engineering. *NPG Asia Mater*, 14: 6.
<https://doi.org/10.1038/s41427-022-00355-x>.
13. Loterie D, Delrot P, Moser C, 2020, High-resolution tomographic volumetric additive manufacturing. *Nat Commun*, 11: 852.
<https://doi.org/10.1038/s41467-020-14630-4>.
14. Thomas A, Orellano I, Lam T, *et al.*, 2020, Vascular bioprinting with enzymatically degradable bioinks via multi-material projection-based stereolithography. *Acta Biomater*, 117: 121–132.
<https://doi.org/10.1016/j.actbio.2020.09.033>.
15. Grigoryan B, Paulsen SJ, Corbett DC, *et al.*, 2019, Multivascular networks and functional intravascular topologies within biocompatible hydrogels. *Science*, 364(6439): 458–464.
<https://www.science.org/doi/10.1126/science.aav9750>.
16. Szklanny AA, Machour M, Redenski I, *et al.*, 2021, 3D bioprinting of engineered tissue flaps with hierarchical vessel networks (VesselNet) for direct host-to-implant perfusion. *Adv Mater*, 33(42): 2102661.
<https://doi.org/10.1002/adma.202102661>.
17. Wu W, DeConinck A, Lewis JA, 2011, Omnidirectional printing of 3D microvascular networks. *Adv Mater*, 23(24): H178–H183.
<https://doi.org/10.1002/adma.201004625>.

18. Kolesky DB, Truby RL, Gladman AS, *et al.*, 2014, 3D bioprinting of vascularized, heterogeneous cell-laden tissue constructs. *Adv Mater*, 26(19): 3124–3130.
<https://doi.org/10.1002/adma.201305506>.
19. Kolesky DB, Homan KA, Skylar-Scott MA, *et al.*, 2016, Three-dimensional bioprinting of thick vascularized tissues. *Proc Natl Acad Sci*, 113(12): 3179–3184.
<https://www.pnas.org/lookup/suppl/doi:10.1073/pnas.1521342113/-/DCSupplemental>.
20. Lin NYC, Homan KA, Robinson SS, *et al.*, 2019, Renal reabsorption in 3D vascularized proximal tubule models. *Proc Natl Acad Sci*, 116(12): 5399–5404.
<https://www.pnas.org/lookup/suppl/doi:10.1073/pnas.1815208116/-/DCSupplemental>.
21. Neufeld L, Yeini E, Reisman N, *et al.*, 2021, Microengineered perfusable 3D-bioprinted glioblastoma model for in vivo mimicry of tumor microenvironment. *Sci Adv*, 7(14): eabi9119.
<https://www.science.org/doi/10.1126/sciadv.abi9119>.
22. Wu C-J, Gaharwar AK, Chan BK, *et al.*, 2011, Mechanically tough pluronic F127/laponite nanocomposite hydrogels from covalently and physically cross-linked networks. *Macromolecules*, 44(20): 8215–8224.
<https://doi.org/10.1021/ma200562k>.
23. Hu M, Dailamy A, Lei XY, *et al.*, 2018, Facile engineering of long-term culturable ex vivo vascularized tissues using biologically derived matrices. *Adv Healthc Mater*, 7(23): 1800845.
<https://doi.org/10.1002/adhm.201800845>.
24. Tocchio A, Tamplenizza M, Martello F, *et al.*, 2015, Versatile fabrication of vascularizable scaffolds for large tissue engineering in bioreactor. *Biomaterials*, 45: 124–131.
<http://dx.doi.org/10.1016/j.biomaterials.2014.12.031>.
25. Li S, Liu Y-Y, Liu L-J, *et al.*, 2016, A versatile method for fabricating tissue engineering scaffolds with a three-dimensional channel for prevasculature networks. *ACS Appl Mater Interfaces*, 8(38): 25096–25103.
<https://doi.org/10.1021/acsami.6b07725>.
26. Yang X, Zhang C, Deng D, *et al.*, 2022, Multiple stimuli-responsive MXene-based hydrogel as intelligent drug delivery carriers for deep chronic wound healing. *Small*, 18(5): 2104368.
<https://doi.org/10.1002/smll.202104368>.
27. Zhang Z, Chen Z, Wang Y, *et al.*, 2019, Bioinspired bilayer structural color hydrogel actuator with multienvironment responsiveness and survivability. *Small Methods*, 3(12): 1900519.
<https://doi.org/10.1002/smt.201900519>.
28. Dabiri SMH, Samiei E, Shojaei S, *et al.*, 2021, Multifunctional thermoresponsive microcarriers for high-throughput cell culture and enzyme-free cell harvesting. *Small*, 17(44): 2103192.
<https://doi.org/10.1002/smll.202103192>.
29. Cui H, Wang W, Shi L, *et al.*, 2020, Superwetable surface engineering in controlling cell adhesion for emerging bioapplications. *Small Methods*, 4(12): 2000573.
<https://doi.org/10.1002/smt.202000573>.
30. Liu M, Wu C, Ke L, *et al.*, 2021, Emerging biomaterials-based strategies for inhibiting vasculature function in cancer therapy. *Small Methods*, 5(7): 2100347.
<https://doi.org/10.1002/smt.202100347>.
31. Downs FG, Lunn DJ, Booth MJ, *et al.*, 2020, Multi-responsive hydrogel structures from patterned droplet networks. *Nat Chem*, 12: 363–371.
<https://doi.org/10.1038/s41557-020-0444-1>.
32. Kan X, Wu C, Wen L, *et al.*, 2020, Biomimetic nanochannels: From fabrication principles to theoretical insights. *Small Methods*, 6(4): 2101255.
<https://doi.org/10.1002/smt.202101255>.
33. Wang X, Yu Y, Yang C, *et al.*, 2021, Microfluidic 3D printing responsive scaffolds with biomimetic enrichment channels for bone regeneration. *Adv Funct Mater*, 31(40): 2105190.
<https://doi.org/10.1002/adfm.202105190>.
34. Li S, Wang W, Li W, *et al.*, 2021, Fabrication of thermoresponsive hydrogel scaffolds with engineered microscale vasculatures. *Adv Funct Mater*, 31(27): 2102685.
<https://doi.org/10.1002/adfm.202102685>.
35. Luo Z, Che J, Sun L, *et al.*, 2021, Microfluidic electro spray photo-crosslinkable κ -Carrageenan microparticles for wound healing. *Eng Reg*, 2: 257–262.
<https://doi.org/10.1016/j.engreg.2021.10.002>.
36. Layek RK, Uddin ME, Kim NH, *et al.*, 2017, Noncovalent functionalization of reduced graphene oxide with pluronic F127 and its nanocomposites with gum arabic. *Compos B Eng*, 128: 155–163.
<https://doi.org/10.1016/j.compositesb.2017.07.010>.
37. Schmidt S, Zeiser M, Hellweg T, *et al.*, 2010, Adhesion and mechanical properties of PNIPAM microgel films and their potential use as switchable cell culture substrates. *Adv Funct Mater*, 20: 3235–3243.
<https://doi.org/10.1002/adfm.201000730>.
38. Zhu CH, Lu Y, Peng J, *et al.*, 2012, Photothermally sensitive poly(N-isopropylacrylamide)/graphene oxide nanocomposite hydrogels as remote light-controlled liquid microvalves. *Adv Funct Mater*, 22(19): 4017–4022.
<https://doi.org/10.1002/adfm.201201020>.

39. Wu L, Pei X, Zhang B, *et al.*, 2022, 3D-printed HAp bone regeneration scaffolds enable nano-scale manipulation of cellular mechanotransduction signals. *J Chem Eng*, 455: 140699.
<https://doi.org/10.1016/j.cej.2022.140699>.
40. Chung TW, Liu DZ, Wang SY, *et al.*, 2003, Enhancement of the growth of human endothelial cells by surface roughness at nanometer scale. *Biomaterials*, 24(25): 4655–4661.
[https://doi.org/10.1016/s0142-9612\(03\)00361-2](https://doi.org/10.1016/s0142-9612(03)00361-2).
41. Cooperstein MA, Canavan HE, 2013, Assessment of cytotoxicity of (N-isopropyl acrylamide) and poly(N-isopropyl acrylamide)-coated surfaces. *Biointerphases*, 8(1): 19.
<https://doi.org/10.1186/1559-4106-8-19>.
42. Xu L, Varkey M, Jorgensen A, *et al.*, 2020, Bioprinting small diameter blood vessel constructs with an endothelial and smooth muscle cell bilayer in a single step. *Biofabrication*, 12(4): 045012.
<https://doi.org/10.1088/1758-5090/aba2b6>.
43. Xie M, Gao Q, Zhao H, *et al.*, 2019, Electro-assisted bioprinting of low-concentration GelMA microdroplets. *Small*, 15(4): 1804216.
<https://doi.org/10.1002/sml.201804216>.
44. Song P, Li M, Zhang B, *et al.*, 2022, DLP fabricating of precision GelMA/HAp porous composite scaffold for bone tissue engineering application. *Compos B Eng*, 244: 110163.
<https://doi.org/10.1016/j.compositesb.2022.110163>.